Cell Reports

Article

Optical regulation of endogenous RhoA reveals selection of cellular responses by signal amplitude

Graphical abstract

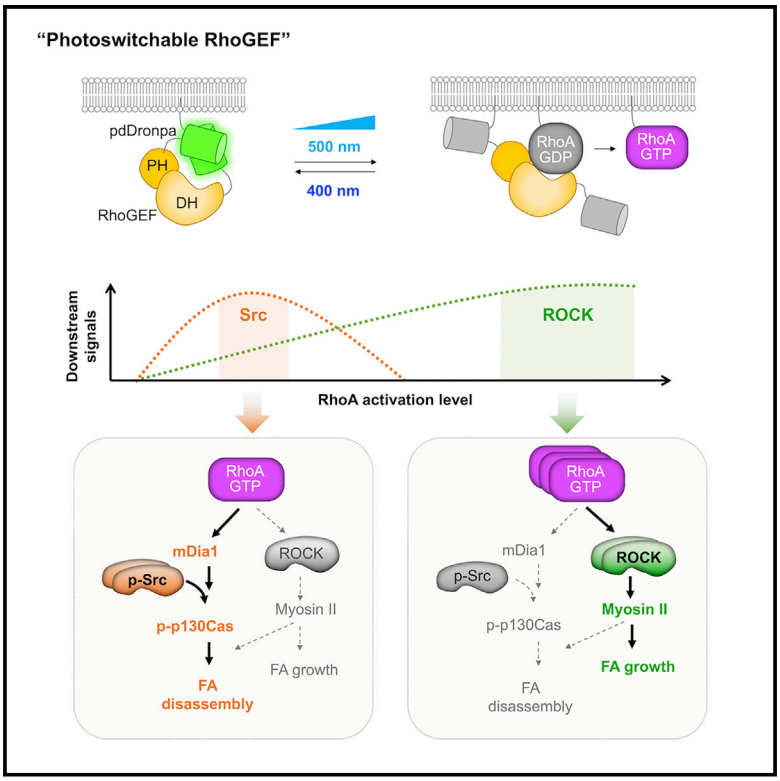

Highlights

- A photoswitchable RhoA GEF enables rheostatic control of endogenous RhoA activity
- Submaximal levels of RhoA activity preferentially induce focal adhesion disassembly
- Src functions as an amplitude-dependent RhoA effector for focal adhesion disassembly
- Amplitude modulation of a single signal can produce distinct cell shape outcomes

Authors

Jeongmin Ju, Hae Nim Lee, Lin Ning, ..., Cherlhyun Jeong, Michael Z. Lin, Jihye Seong

Correspondence

mzlin@stanford.edu (M.Z.L.), jseong@kist.re.kr (J.S.)

In brief

Ju et al. develop photoswitchable RhoA GEF that enables rheostatic control of endogenous RhoA activity. Fine modulation of RhoA signal amplitude reveals that submaximal levels of RhoA activity preferentially induce focal adhesion disassembly through selective activation of Src kinase, suggesting that amplitude of a single signal can produce distinct cell outcomes.

Ju et al., 2022, Cell Reports *40*, 111080
July 12, 2022
https://doi.org/10.1016/j.celrep.2022.111080

CellPress

Cell Reports

CellPress
OPEN ACCESS

Article

Optical regulation of endogenous RhoA reveals selection of cellular responses by signal amplitude

Jeongmin Ju,[1,2,7] Hae Nim Lee,[1,3,7] Lin Ning,[4,5] Hyunjoo Ryu,[1] Xin X. Zhou,[4,5] Hyeyeon Chun,[1] Yong Woo Lee,[1] Austin I. Lee-Richerson,[4] Cherlhyun Jeong,[6] Michael Z. Lin,[4,5,*] and Jihye Seong[1,2,3,4,8,*]

[1]Brain Science Institute, Korea Institute of Science and Technology, Seoul 02792, Republic of Korea
[2]Division of Bio-Medical Science & Technology, KIST School, Korea University of Science and Technology, Seoul 02792, Republic of Korea
[3]Department of Converging Science and Technology, Kyung Hee University, Seoul 02453, Republic of Korea
[4]Department of Bioengineering, Stanford University, Stanford, CA 94305, USA
[5]Department of Neurobiology, Stanford University, Stanford, CA 94305, USA
[6]Center for Theragnosis, Korea Institute of Science and Technology, Seoul 02792, South Korea
[7]These authors contributed equally
[8]Lead contact
*Correspondence: mzlin@stanford.edu (M.Z.L.), jseong@kist.re.kr (J.S.)
https://doi.org/10.1016/j.celrep.2022.111080

SUMMARY

How protein signaling networks respond to different input strengths is an important but poorly understood problem in cell biology. For example, RhoA can promote focal adhesion (FA) growth or disassembly, but how RhoA activity mediates these opposite outcomes is not clear. Here, we develop a photoswitchable RhoA guanine nucleotide exchange factor (GEF), psRhoGEF, to precisely control endogenous RhoA activity. Using this optical tool, we discover that peak FA disassembly selectively occurs upon activation of RhoA to submaximal levels. We also find that Src activation at FAs selectively occurs upon submaximal RhoA activation, identifying Src as an amplitude-dependent RhoA effector. Finally, a pharmacological Src inhibitor reverses the direction of the FA response to RhoA activation from disassembly to growth, demonstrating that Src functions to suppress FA growth upon RhoA activation. Thus, rheostatic control of RhoA activation by psRhoGEF reveals that cells can use signal amplitude to produce multiple responses to a single biochemical signal.

INTRODUCTION

A fundamental question in cellular computation is whether different activation levels of a single biochemical signal can be used to generate distinct functional outputs. For example, overexpression of individual members of the Rho family of guanosine triphosphate (GTP) hydrolases (GTPases) induces specific actin-based structures, with Cdc42 promoting filopodium formation and extension, Rac1 lamellipodium formation and extension, and RhoA actinomyosin contractility (Nobes and Hall, 1995). However, experiments with fluorescent reporters have shown that, even within the same cell, individual GTPases are activated at sites and times of seemingly opposite morphological responses. For instance, in migrating cells, RhoA is activated at the leading edge, which is extending, and at the lagging edge, which is retracting (Heasman and Ridley, 2010; Machacek et al., 2009; Pertz et al., 2006; Wong et al., 2006). Similarly, RhoA is required for focal adhesion (FA) growth in response to various extracellular stimuli (Nobes and Hall, 1995; Parsons et al., 2010) but has also been implicated in the reverse process of FA disassembly (Lock et al., 2012; Yamana et al., 2006). Given its apparent involvement in induction of opposing morphological changes, RhoA signaling to FAs could serve as a model system for understanding how a single regulatory protein can produce divergent downstream effects.

Although mechanisms from RhoA to FA assembly have been extensively studied (Nobes and Hall, 1995; Parsons et al., 2010), much less is known about the mechanisms linking RhoA to FA disassembly. FA formation is a reliable static outcome of many extracellular stimuli, but FA disassembly has been studied primarily in the context of cell migration, when FAs are continuously assembled and disassembled (Parsons et al., 2010). Indeed, localized FA disassembly allows cell regions to detach from their environment and, thus, is of essential importance in cell migration and cancer metastasis (Carragher and Frame, 2004). RhoA has been hypothesized to drive lagging edge retraction based on biosensor imaging in migrating cells (Heasman and Ridley, 2010; Wong et al., 2006), but it is unclear whether RhoA is responsible for FA disassembly during this process or how such a function would be reconciled with the better understood function of RhoA in FA growth.

Global loss-of-function techniques have been used to study RhoA effectors in FA disassembly, but it is difficult to dissociate primary from secondary phenotypes in such experiments.

For example, dominant-negative constructs, RNAi, or chemical inhibitors of the mDia and Rho-associated protein kinase (ROCK) families of RhoA effectors (hereafter referred to collectively as mDia and ROCK) produce trailing edge phenotypes in migrating cells, suggesting functions in FA disassembly (Lock et al., 2012; Webb et al., 2004; Yamana et al., 2006). However, these global manipulations disrupt protein function throughout the cell over long periods of time, and mDia and ROCK also have well-characterized roles in FA assembly and growth at the leading edge (Amano et al., 1997; Burridge and Guilluy, 2016; Meenderink et al., 2010; Oakes et al., 2012; Stricker et al., 2013; Wolfenson et al., 2011). Any observed deficits in FA disassembly in migrating cells upon interference with mDia or ROCK function could thus be secondary to earlier deficits in FA growth at the leading edge.

To clearly elucidate molecular mechanisms governing cell responses to specific protein activities, such as FA disassembly in response to RhoA, a method to activate a specific protein separately from other signaling pathways at a particular time would be useful (Seong and Lin, 2021). Here we report the engineering of a photoswitchable activator of endogenous RhoA, psRhoGEF. We also develop a RhoA biosensor based on fluorescence resonance energy transfer (FRET) with LSSmOrange and mKate2 as a FRET pair to measure the RhoA activity induced by psRhoGEF without spectral overlapping. By applying different doses of light to psRhoGEF for rheostatic RhoA activation, we find that RhoA activation induces FA disassembly in an amplitude-dependent manner, peaking at submaximal levels of RhoA activity. This RhoA-induced FA disassembly is dependent on Src activation at FA because we observe that Src activation at FAs occurs preferentially at lower levels of RhoA activation, which also confirmed by FRET-based Src biosensors. Inhibition of Src-family kinases promotes FA growth in response to RhoA activation. These results thus elucidate a specific role of Src in RhoA-induced FA disassembly and explain how a biochemical signal can produce opposite outcomes depending on signal amplitude and context. Our results also demonstrate how new optical control of protein activity overcomes limitations of traditional methods in investigating complex cellular behaviors.

RESULTS

Strategies for optical control of endogenous RhoGTPases

Two general types of strategies have been devised previously for optical control of Rho-family GTPase activity. The first strategy involves expressing optically controllable forms of the Rho-family GTPase itself. For example, RhoA fused to cryptochrome 2 (CRY2) is clustered by blue light, resulting in its activation by unknown mechanisms (Bugaj et al., 2013). Alternatively, RhoA can be sequestered to mitochondria via a protein-protein interaction that occurs in the dark but not in blue light so that it can be released throughout the cell upon illumination (Wang et al., 2016). In another example, RhoA can be fused to BcLOV4 (Berlew et al., 2021), a light-oxygen-voltage (LOV) domain that interacts with phospholipid membranes after illumination. Light allows the RhoA-BcLOV4 protein to accumulate at the plasma membrane, leading to RhoA activation (Glantz et al., 2018, 2019). Finally, although not yet demonstrated for RhoA control, a precisely optimized fusion of a LOV domain to the N terminus of Rac1 GTPase blocked its ability to interact with effectors until illuminated (Wu et al., 2009).

However, this class of strategies involves introduction of exogenous RhoA over a background of endogenous expression. This is a problem because addition of more copies of a Rho-family GTPase can lead to unnatural phenotypes; e.g., by overwhelming mechanisms that target endogenous GTPases to specific subcellular locations or by sequestering regulators such as Rho guanine nucleotide dissociation inhibitors (GDIs), which are expressed at limited concentrations (Michaelson et al., 2001). Specifically, it has been demonstrated that expression of any Rho-family GTPase (Cdc42, Rac, and RhoA) competes with endogenous Rho-family GTPases for binding to RhoGDI-family proteins. Because RhoGDIs sequester the guanosine diphosphate (GDP)-bound fraction of Rho-family GTPases and protect them from degradation (Figure S1A), introduction of exogenous Rho GTPases results in reduced levels of endogenous GTPases and constitutive activation of the remaining fraction (Boulter and Garcia-Mata, 2010; Bozza et al., 2015; Figure S1B). Thus, introducing additional GTPase molecules can produce artifactual effects on cellular behavior.

A different strategy that may produce fewer artifactual results is to use light to control upstream activators of endogenous Rho-family GTPases rather than introducing exogenous fusion proteins of the GTPases themselves. Naturally, Dbl-family guanine nucleotide exchange factors (GEFs) constitute the primary means by which cells regulate the activity of each Rho-family GTPase (Luo, 2000; Machacek et al., 2009). Various Dbl-family GEFs catalyze activation of specific Rho-family GTPases by converting the inactive GDP-bound to the active GTP-bound form, which then binds to and activates downstream effectors (Rossman et al., 2005). Indeed, RhoA function has been optically modulated by using light-induced heterodimeric interactions such as the N-terminal of Cry-interacting basic helix-loop-helix protein 1 (CRY2-CIBN) to increase the concentrations of a RhoGEF at the plasma membrane, where the functional subpopulation of RhoA resides (O'Neill et al., 2016; Valon et al., 2017; Wagner and Glotzer, 2016). However, this involves overexpression of an active form of a RhoGEF throughout the cytosol, which may cause a nonspecific effect prior to light-induced membrane recruitment (Valon et al., 2017).

Alternatively, a single-chain photoswitchable GEF can be made by fusing a GEF catalytic domain to two copies of a photodissociable variant of the green fluorescent protein Dronpa (pdDronpa) so that the active site is caged in the dark (Zhou et al., 2012, 2017). Cyan light induces dissociation of the fluorescent protein domains and restoration of GEF activity, after which violet light can induce fluorescent protein domain re-association and protein re-caging. This process is reminiscent of the natural activation mechanism of some GEFs, in which an upstream signal induces release of an intramolecular inhibitory interaction (Rossman et al., 2005). By avoiding overexpression of RhoA and the resulting titration of RhoGDIs stabilizing endogenous Rho-family GTPases, this strategy may preserve more native-like signaling states (Figure S1C).

Development of a photoswitchable GEF for RhoA

We thus set out to construct a photocontrollable RhoA GEF. A photoswitchable Cdc42 GEF (psCdc42GEF) has been constructed previously by fusing photodissociable dimeric Dronpa (pdDronpaM) fluorescent protein domains to each end of the Dbl-homology (DH) domain of intersectin, followed by a CAAX sequence for localization to the plasma membrane (Zhou et al., 2012, 2017). Baseline dimerization of pdDronpa sterically blocks the intersectin active site, whereas illumination causes pdDronpa dissociation and allows intersectin to bind to and activate Cdc42 (Zhou et al., 2012, 2017). We investigated whether this design could be generalized by creating a photoswitchable RhoA GEF based on the RhoA-specific activator PDZ (post-synaptic density protein, Drosophila disc large tumor suppressor, and zonula occludens-1 protein) RhoGEF (PRG) (Jaiswal et al., 2011; Oleksy et al., 2006; Figures 1A and 1B).

Previous *in vitro* findings mapped specificity determinants to only the PRG DH domain (Oleksy et al., 2006), so we first tested constructs in which photodissociable Dronpa domains (tetrameric DronpaN or dimeric pdDronpaM) (Zhou et al., 2012, 2017) were attached to both termini of the PRG DH domain, similar to psCdc42GEF. However, HEK293A cells expressing these constructs produced a variety of responses to light, including filopodium formation and cell spreading (Figure 1C), suggestive of nonspecific responses from Cdc42 and Rac activation. These findings indicated that the DH domain alone in PRG is not sufficient to impart specificity for RhoA over other GTPases in cells, in contrast to the DH domain of the Cdc42 GEF intersectin.

We thus explored whether other elements in PRG could confer RhoA specificity in cells. Although intersectins (ITSNs) specifically bind to their substrates using only the DH domain (Snyder et al., 2002), the crystal structure of the RhoA-PRG complex shows the DH and pleckstrin homology (PH) domains of PRG contacting RhoA (Bielnicki et al., 2011; Kristelly et al., 2004; Figure 1A). In addition, a "GEF switch" sequence immediately upstream of the PRG DH domain has also been suggested to interact with RhoA and contribute to its activation (Bielnicki et al., 2011). Indeed, constructs in which the GEF switch sequence, DH domain, and PH domain were flanked by photodissociable dimeric Dronpa (pdDronpaM or its higher-affinity derivative pdDronpaV) (Zhou et al., 2017; Figure 1B) demonstrated RhoA-specific effects upon illumination (Figure 1C). Finally, we optimized linker lengths while testing the photodissociable pairs of pdDronpaV-pdDronpaV, pdDronpa1-pdDronpa1, and pdDronpa1-pdDronpa1 N145K (Figure 1D), which form a series with decreasing affinity (Zhou et al., 2017). pdDronpaV-PRG DHPH-GSS_1-pdDronpaV was most reliable in inducing cell contraction (Figure 1D) and was designated psRhoGEF (Figures 1B and 1E). psRhoGEF-induced acute RhoA activation resulted in strong cellular contraction in HEK293A cells (Figure 1F; Video S1). We further confirmed, by Rho GTPase pull-down assay, that different light doses on psRhoGEF can induce different levels of RhoA activation (Figure 1G).

For comparison, we also tested two other optobiochemical systems for RhoA activation, OptoGEF-RhoA (Valon et al., 2017) and photo-recruitable (PR)-GEF (Wagner and Glotzer, 2016). In OptoGEF-RhoA, a light-induced CRY2-CIBN interaction can increase the concentration of the functional domains of PRG in the plasma membrane (Valon et al., 2017), and in PR-GEF, the PDZ-LOVpep interaction recruits the DH domain of leukemia-associated RhoGEF (LARG) to the plasma membrane, thus allowing both to activate RhoA (Wagner and Glotzer, 2016; Figure S2A). OptoGEF-RhoA and PR-GEF mediated cell shrinkage upon illumination (Figure S2B). Thus, all three optobiochemical systems functioned effectively. One point of difference between the systems was reversibility; after illumination was terminated, the light-induced localization of PR-GEF and OptoGEF-RhoA immediately reversed (Figures S2C–S2D). In contrast, psRhoGEF remained in its uncaged conformation, but 400 nm of illumination immediately returned it to its caged state (Figures S2E–S2F). psRhoGEF was less affected by expression conditions in our hands, and its single-chain nature simplified co-expression with other constructs.

Development of a RhoA FRET biosensor compatible with psRhoGEF

To examine RhoA activity in living cells expressing psRhoGEF, we created a RhoA FRET biosensor that could be imaged without interference by the cyan light used to activate psRhoGEF. The large-Stokes-shift orange fluorescent protein LSSmOrange and the far-red mKate2 are an appropriate FRET pair; they are minimally excited at the 500-nm wavelengths used to induce psRhoGEF (Figures 2A and 2B). Thus we created a RhoA biosensor composed of LSSmOrange, the rhotekin RBD, a long linker, mKate2, and RhoA (Figure 2A), modifying a previous design that had used cyan and yellow fluorescent proteins (Fritz et al., 2013).

To test the activity and specificity of our RhoA biosensor, we compared FRET levels in cells expressing ITSN-DH, Tiam-DH, or PRG-DHPH. FRET was significantly higher in cells expressing the PRG-DHPH domain (Figures 2C and 2D), indicating that this sensor responds to RhoGEF with increased FRET (Figure 2A). In contrast, the biosensor did not respond to ITSN-DH or Tiam-DH domains (Figures 2C and 2D), confirming specificity for activation by RhoGEFs. The RhoA biosensor also responds in the presence of Dronpa; we observed that the FRET level of this biosensor in cells expressing PRG DHPH fused to a monomeric Dronpa domain, DronpaK, was significantly higher than in cells expressing DronpaK only (Figure 2E). We also generated constitutively active or inactive biosensors by introducing G14V or T17N mutations in the RhoA of the biosensor, respectively, and, as expected, the RhoA G14V biosensor exhibited a higher FRET level than the RhoA T17N biosensor (Figures 2F–2H).

We next determined whether this RhoA FRET biosensor can report RhoA activation by psRhoGEF in live cells. When the RhoA biosensor was coexpressed with psRhoGEF (Figure 3A), we observed a FRET increase of the RhoA biosensor after illumination on psRhoGEF (Figures 3B and 3C). We also found that psRhoGEF with an inactivating R868G mutation (Jaiswal et al., 2011; Oleksy et al., 2006) failed to induce a FRET response upon illumination (Figures 3B and 3C), confirming that biosensor induction upon psRhoGEF photoillumination required psRhoGEF enzymatic activity. Next we introduced the wild-type (WT) biosensor or negative mutant T17N biosensor together with psRhoGEF. As expected, illumination caused increased FRET in

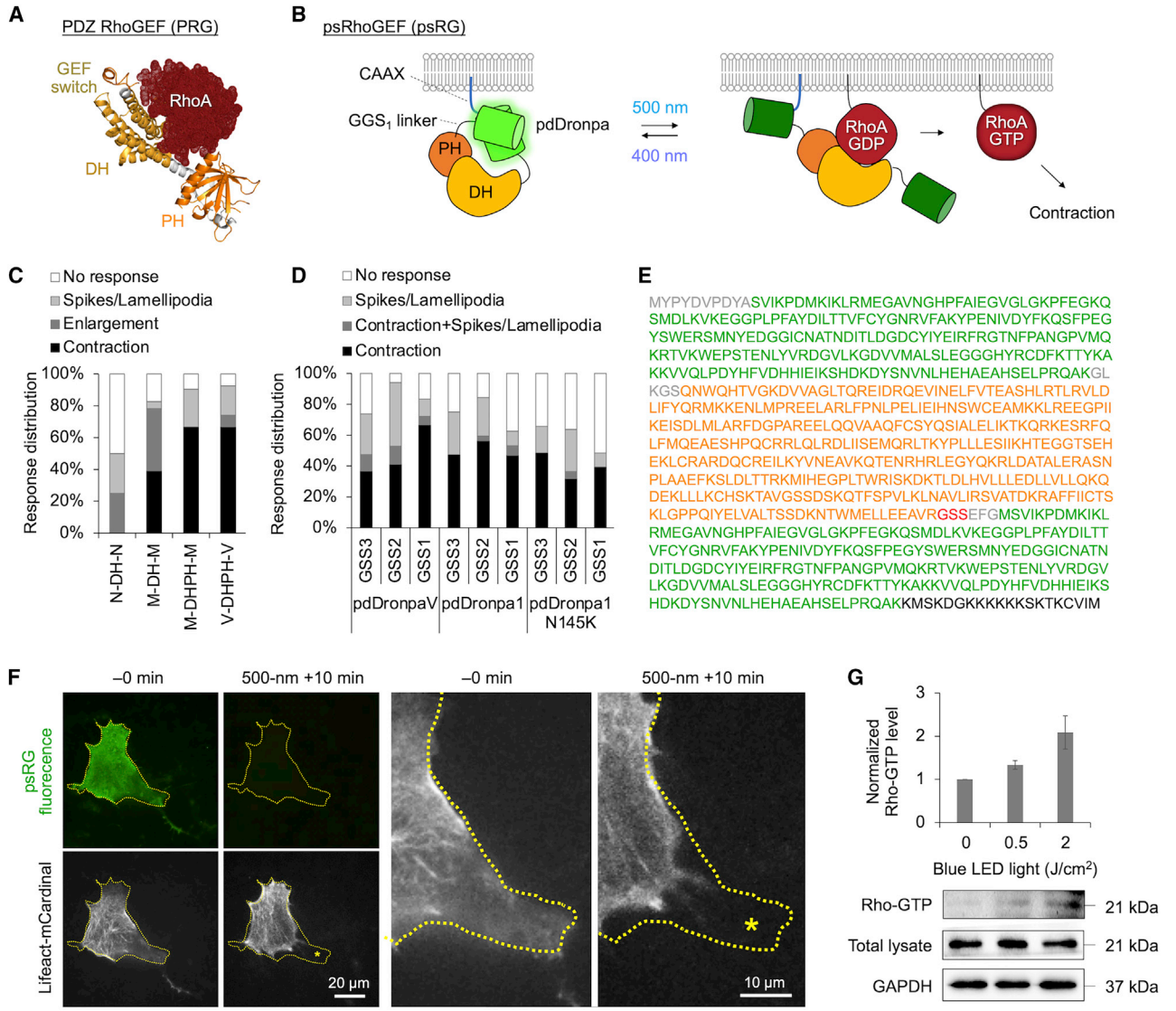

Figure 1. Design and validation of photoswitchable RhoGEF

(A) Co-crystal structure of PDZ RhoGEF (PRG) and RhoA (PDB: 3T06).

(B) Photoswitchable RhoGEF comprises the PRG RhoA-interacting regions (GEF switch, DH domain, and PH domain) fused to a pdDronpaV domain at each end with a C-terminal CAAX sequence.

(C) Distribution of responses to cyan illumination (11 J/cm^2) by time-lapse microscopy of cells expressing psRhoGEF candidates. The designs tested were the PRG DH domain only fused at each end to DronpaN or pdDronpaM on both termini with the right-side linker GSS_4 (n = 8 and 23) and the PRG DHPH domain fused at each end to pdDronpaM or pdDronpaV on both termini with the right-side linker GSS_3 (n = 21 and 27).

(D) Distribution of responses to cyan illumination (11 J/cm^2) in cells expressing psRhoGEF candidates, comprising PRG DHPH fused at each end to Dronpa variants with various right-side linker lengths. The designs tested were pdDronpaV on both termini with the right-side linker GSS_1 (n = 18), GSS_2 (n = 17), or GSS_3 (n = 19); pdDronpa1 on both termini with the right-side linker GSS_1 (n = 32), GSS_2 (n = 32), or GSS_3 (n = 40); and pdDronpa1 on the N-terminus and pdDronpa1 N145K on the C-terminus with the right-side linker GSS_1 (n = 33), GSS_2 (n = 22), or GSS_3 (n = 33).

(E) psRhoGEF sequence, colored as follows: gray, epitope tag or restriction enzyme site; green, pdDronpaV; orange, GEF switch, DH and PH domains from PRG; red, GSS_1 linker; black, CAAX signal.

(F) Fluorescence of pdDronpa in psRhoGEF and Lifeact-mCardinal before and after 500-nm illumination. Right: enlarged view of the retracting edge. Dotted line, original cell outline; asterisk, retracted region. Scale bars, 20 or 10 μm.

(G) Dose-dependent RhoA activation in psRhoGEF-expressing cells by RhoA-GTP pull-down (n = 4). Blue light-emitting diode (LED) light was applied at the indicated energy densities. Error bars indicate standard error of the mean (SEM).

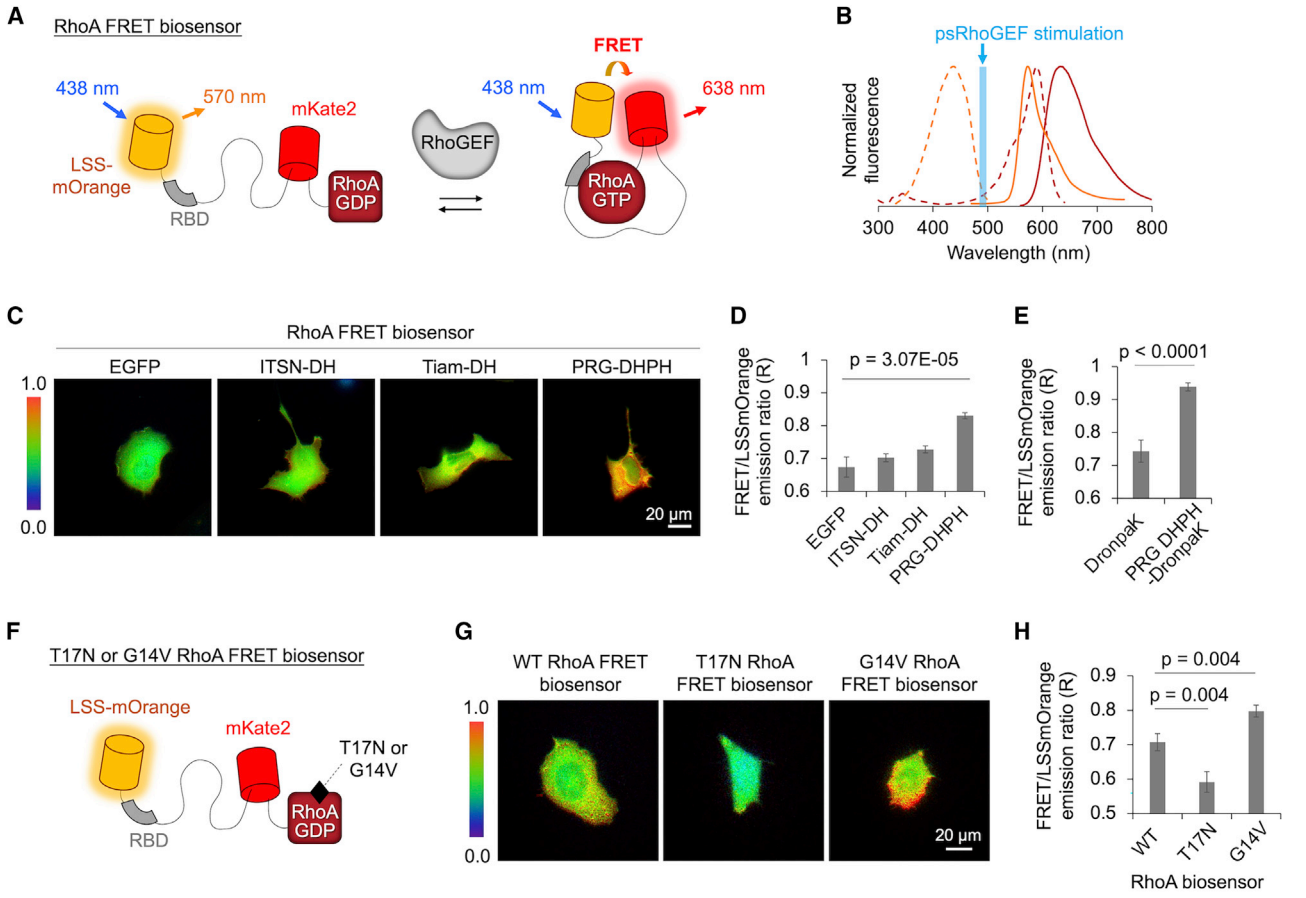

Figure 2. The RhoA biosensor with LSSmOrange/mKate2 as a FRET pair

(A) Schematic of the design of a RhoA biosensor with a FRET pair, LSSmOrange and mKate2.

(B) Spectral profile of LSSmOrange and mKate2. Orange lines present the profile of LSSmOrange, and dark red lines show the profile of mKate2. The dotted and solid lines are excitation and emission spectra, respectively. The cyan line shows the peak excitation wavelength of Dronpa for stimulation of psRhoGEF.

(C and D) Representative images (C) and average levels of FRET/LSSmOrange emission ratios (D) in cells expressing the RhoA biosensor together with p2A-EGFP, EGFP-p2A-ITSN-DH, EGFP-p2A-Tiam-DH, or EGFP-p2A-PRG-DHPH domains (n = 26, 52, 64, or 90; p values were calculated by two-tailed Student's t test). Scale bar, 20 μm.

(E) Mean FRET/LssmOrange emission ratios in cells expressing the RhoA biosensor together with DronpaK or DronpaK-PRG DHPH (n = 13 and 18; p values were calculated by two-tailed Student's t test).

(F) RhoA biosensor mutants containing dominant-negative (T17N) or constitutively active mutant (G14V) RhoA.

(G) Representative images of FRET/LSSmOrange emission ratios in cells expressing WT RhoA, T17N RhoA, or the G14V RhoA FRET biosensor. Scale bar, 20 μm.

(H) Mean FRET/LSSmOrange emission ratios in cells expressing WT RhoA, dominant-negative T17N RhoA, or the constitutively active G14V RhoA biosensor. Statistical significance was calculated by two-tailed Student's t test (n = 37, 35, or 40). In all panels, error bars indicate SEM.

the WT but not T17N biosensor (Figure S3). These results confirmed that the FRET response can report RhoA activation induced by illumination of psRhoGEF in living cells.

The RhoA FRET biosensor can report different levels of RhoA activation induced by illumination of different light intensities on psRhoGEF (Figures 3D and 3E). When psRhoGEF is activated by illumination, the intensity of Dronpa decreases (Figure 3A); thus, we can also observe that the decrease in Dronpa intensity depended on the light doses (Figure 3F). Thus, the RhoA FRET biosensor can report the amplitude of RhoA activation induced by psRhoGEF. The RhoA biosensor also confirmed that Dronpa intensity upon illumination can represent the RhoA activation states.

Dose-dependent effects of RhoA activation on FA dynamics

RhoA has well-established functions in promoting FA formation, but its potential role in FA disassembly is less clear. Following early observations that microinjection of RhoA induces FA formation in confluent fibroblasts (Nobes and Hall, 1995), multiple experiments have established that RhoA and its effectors are required for FA induction by extracellular stimuli such as LPA or growth factors (Amano et al., 1997; Oakes et al., 2012; Ridley et al., 1992). If FA disassembly is considered the reverse of FA assembly, then it might be expected that RhoA activation would inhibit FA disassembly. Indeed, chronic activation of RhoA has been found to inhibit FA disassembly in fibroblasts, whereas

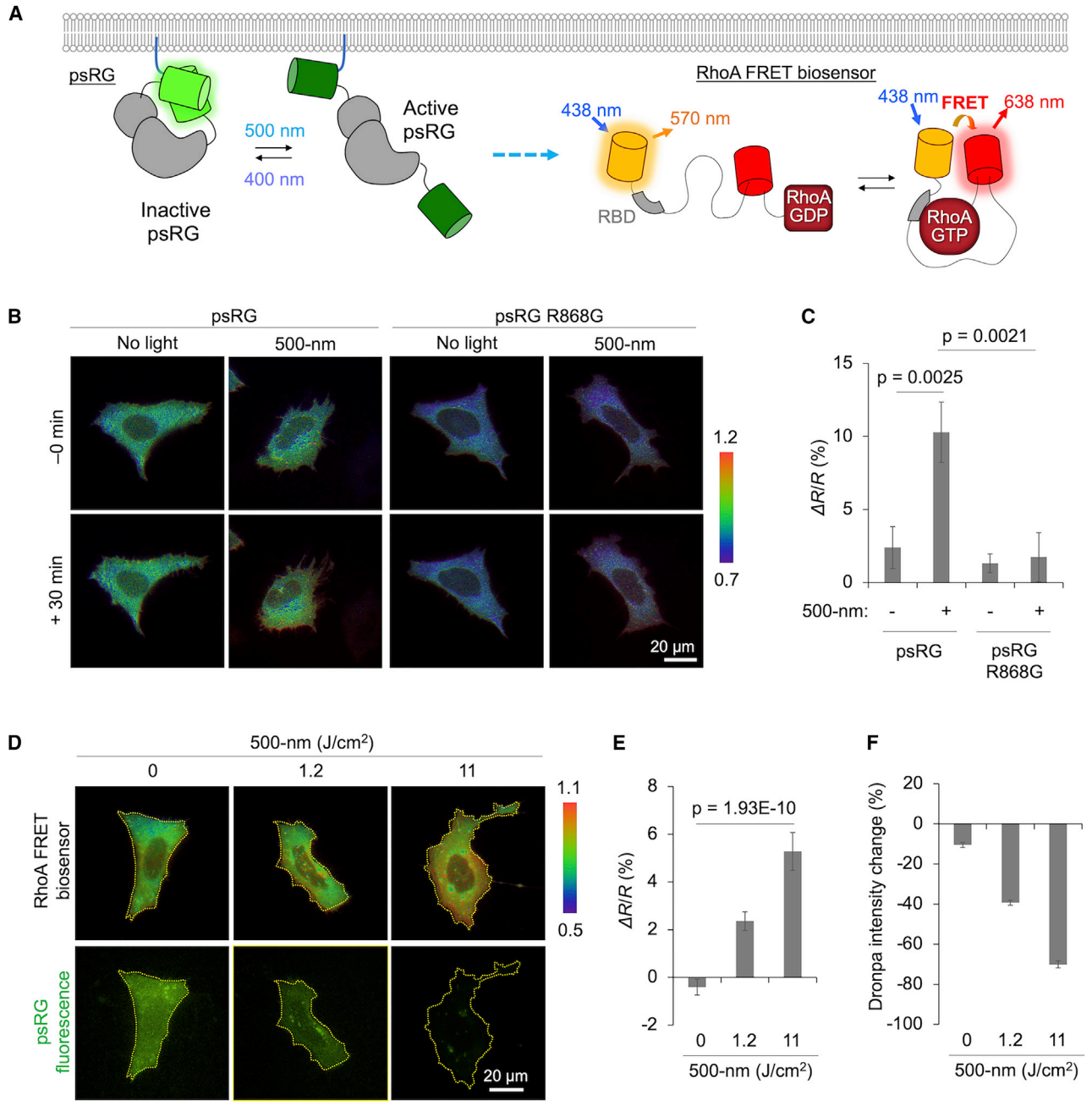

Figure 3. A FRET biosensor reports RhoA activation by illuminated psRhoGEF

(A) Schematic of FRET-based measurement of psRhoGEF-induced RhoA activation.

(B and C) Representative images (B) and quantification (C) showing the changes in FRET ratios with or without cyan illumination (11 J/cm^2) in cells co-expressing psRhoGEF or the psRhoGEF R868G mutant (n = 22, 42, 14, or 21). Statistical significance is calculated by two-tailed Student's t test. Scale bar, 20 μm.

(D–F) Representative images (D) and changes in FRET ratios of the RhoA biosensor (E) in cells expressing psRhoGEF without or with different light doses of illumination ($p = 1.9 \times 10^{-10}$ by one-way ANOVA; n = 36, 38, or 34). Scale bar, 20 μm.

(F) The corresponding Dronpa intensity changes of psRhoGEF are shown for the indicated groups (n = 36, 38, or 34).

Error bars indicate SEM.

chronic inhibition of RhoA induced FA disassembly (Ren et al., 2000). Acute pharmacological inhibition of ROCK or myosin II, which is activated by ROCK, induces FA disassembly (Seong et al., 2013; Wolfenson et al., 2011), consistent with a role of myosin in maintaining FAs. On the other hand, other experiments suggest a function of RhoA activation in FA disassembly with faster kinetics. Microinjection of RhoA induces rapid contraction of subconfluent fibroblasts (Paterson et al., 1990). We also

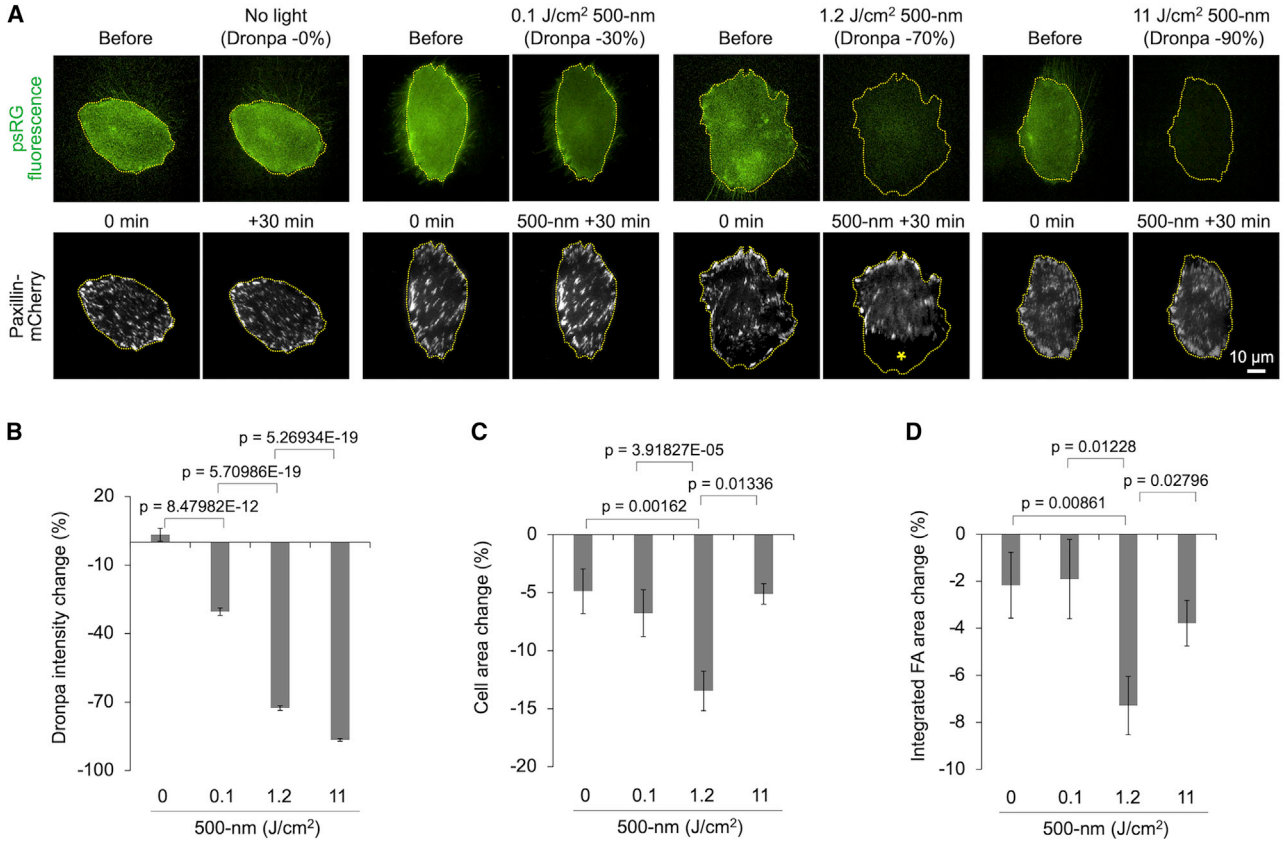

Figure 4. Dose-specific effect of psRhoGEF on FA responses

(A) Representative psRhoGEF and paxillin-mCherry images before and after illumination with different light doses in U87-MG cells stably expressing psRhoGEF. Scale bar, 10 μm.

(B) Intensity changes of Dronpa in U87-MG cells stably expressing psRhoGEF without or with different doses of illumination (n = 20, 36, 56, 85).

(C and D) The changes in cell size (C) and total FA area (D) in U87-MG cells stably expressing psRhoGEF at a 30-min interval without or with different doses of illumination (n = 20, 36, 56, 85). Focal adhesion (FA) area was calculated using the Focal Adhesion Analysis Server (FAAS) (Berginski and Gomez, 2013). Statistical significance is calculated by two-tailed Student's t test.

Error bars indicate SEM.

observed that photoinduction of psRhoGEF induced rapid shrinkage of subconfluent HEK293A cells (Figure 1F).

We hypothesized that acute RhoA activation can induce FA disassembly during cell retraction. To test this, we first generated a stable cell line in U87-MG astrocytoma cells with psRhoGEF-containing lentiviruses and visualized FAs with mCherry-tagged paxillin before and after illumination with 500-nm light. As we hypothesized, acute RhoA activation can induce FA disassembly at the retracted region (Video S2) but, interestingly, in a dose-specific manner (Figure 4). Illumination with 0.1 J/cm^2 cyan light turns off ~30% of the Dronpa fluorescence in psRhoGEF, but no significant FA change was observed (Figure 4). However, efficient FA disassembly was detected after 1.2 J/cm^2 cyan light, which turns off ~70% of Dronpa fluorescence (Figure 4). Unexpectedly, we found that RhoA-mediated FA disassembly is less frequent with a stronger light dose of 11 J/cm^2, corresponding to switching off 90% of Dronpa (Figure 4). In addition, localized FA growth could be observed in some cells (Figure S4A), although the net FA response in cells was still disassembly (Figure 4D).

To assure that these dose-specific FA changes were not due to light alone, we also examined DronpaK-expressing cells after illumination. These cells showed no changes in total cell area or total FA area at each light dose (Figures S4B–S4D). To confirm the results in psRhoGEF-expressing cells with a different FA marker, we also performed experiments with mCherry-tagged vinculin. mCherry-tagged vinculin also revealed that moderate, not high, levels of psRhoGEF activation were optimal for FA disassembly (Figure S5).

To confirm that this effect is due to RhoA activation and independent of the optical control system, we also performed RhoA activation by photoinduction of PR-GEF. We found that RhoA-induced cell contraction and FA disassembly were again most efficiently observed after the medium dose of light stimulation on PR-GEF (Figure S6). This confirms our finding that submaximal levels of RhoA activity selectively induce FA disassembly. The LOV switch in PR-GEF is sensitive to low doses of light. Thus, rather than using different amounts of light, we applied different duty cycles (short lit intervals alternating with dark intervals). Compared with LOV domains, the relatively lower

quantum yield of photoswitching in pdDronpa (Zhou et al., 2017) facilitates rheostatic activation of psRhoGEF levels by applying different instantaneous powers of light for true amplitude modulation.

Use of optically controllable RhoA activators thus reveals, unexpectedly, that acute submaximal RhoA activation is most efficient in inducing FA disassembly and cell contraction.

RhoA-mediated FA disassembly is dependent on Src activation at FAs

We next investigated the downstream signaling pathways mediating this dose-dependent function of RhoA on FA dynamics. One effector of RhoA is mDia1, which mediates recruitment to FAs of Src kinase (Yamana et al., 2006), whose activity is necessary for FA disassembly in migrating cells (Carragher and Frame, 2004; Yamana et al., 2006). Src phosphorylation of the FA components p130Cas and cortactin has been shown to accelerate their dissociation from FAs and to be required for FA turnover in migrating cells (Machiyama et al., 2014; Sawada et al., 2006; Wang et al., 2011).

We thus investigated the effect of different RhoA levels on Src activity at FAs after illumination of psRhoGEF-expressing cells with different light doses. Performing immunostaining for Src autophosphorylation at Tyr-416, we observed colocalization of p-Src and paxillin-mCherry after illumination by 1 J/cm^2 cyan light (Figure 5A), suggesting that psRhoGEF can induce the Src activation at FAs. p-Src colocalization was lower after 5 J/cm^2 illumination (Figure 5A), implying that a high level of RhoA activation is not optimal for Src activation at FAs.

We designed a FRET-based Src biosensor compatible with psRhoGEF by replacing the enhanced cyan/yellow fluorescent protein (ECFP/YPet) pair of the previously developed membrane-targeted Src biosensor, called the Lyn-Src biosensor (Seong et al., 2009, 2011), with LSSmOrange and mKate2 (Figure 5B). After validating that the emission ratio of FRET/LSSmOrange can represent the Src activity in live cells (Figure S7; Video S3), we applied different light doses to cells expressing psRhoGEF and the FRET-based Src biosensor. Again, we observed local Src activation at contracting cell edges when ~70% of Dronpa fluorescence in psRhoGEF was turned off by 1.2 J/cm^2 cyan light (Figures 5C–5E). In contrast, local Src activation was not observed after 11 J/cm^2 cyan light and 90% Dronpa off-switching (Figures 5C–5E).

These results suggest that RhoA-mediated FA disassembly may depend on dose-specific Src activation at FAs. To test this hypothesis, we examined the effects of perturbing Src activity on the response of FAs to different levels of RhoA activation. Indeed, FA disassembly induced by 1.2 J/cm^2 cyan light on psRhoGEF was completely prevented by pretreatment with the Src inhibitor PP2 (Figure 5F). In the context of high-dose (11 J/cm^2) activation of psRhoGEF, PP2 or dominant-negative Src K295R enhanced centripetal growth of some FAs while maintaining their attachment (Figures 5G and S8A; Video S4), resulting in increased FA area per cell (Figure 5H). In contrast, augmenting Src activity with constitutively active Src Y527F during strong RhoA activation resulted in faster cell shrinkage and FA disassembly (Figures S8B-S8C). Thus, Src inhibition switches outcomes of moderate RhoA activation to FA growth, whereas Src enhancement switches outcomes of high RhoA activation to FA disassembly.

These results demonstrate that moderate levels of RhoA activity specifically enhance Src activity at FAs, which then drives FA disassembly.

ROCK activity is required for FA assembly and disassembly

Activated RhoA induces activation of the Rho-associated protein kinase ROCK. We thus measured ROCK activation at different light doses by phospho-ROCK immunostaining. As expected, higher light doses applied on psRhoGEF induced stronger ROCK activation (Figure 6A). We also observed increased actin stress fibers and phosphorylation of myosin light chain (MLC), which are downstream of ROCK, in a dose-dependent manner (Figure S9). ROCK has well-established functions as a RhoA effector mediating FA assembly and maturation (Burridge and Guilluy, 2016). Indeed, we observed that FA size is significantly reduced in cells treated with the ROCK inhibitor Y-27632 (Figure 6B), confirming the role of ROCK in FA assembly.

We then wanted to determine whether ROCK activity is required for the FA disassembly observed after 1.2 J/cm^2 illumination of psRhoGEF. Time-lapse imaging of FA disassembly after RhoA activation revealed centripetal stretching of FAs prior to their removal (Video S4), suggesting a role of actin contractility, which ROCK promotes through myosin II activation (Amano et al., 2010). Indeed, inhibition of ROCK by Y-27632 inhibited FA disassembly downstream of moderate RhoA activation (Figures 6C and 6D), consistent with a role of contractility in FA disassembly. However, because FAs are already small after Y-27632 treatment, we cannot rule out that the remaining paxillin signals label FA core elements that resist disassembly. FA responses after 11 J/cm^2 of illumination of psRhoGEF were also not noticeably altered by ROCK inhibition (Figure 6E). This is consistent with ROCK not simply counteracting Src-mediated disassembly at higher RhoA levels, but, again, the small FAs that remain after Y-27632 treatment may not be able to respond by further disassembly.

Our results suggest a model for how different levels of RhoA activation induce different downstream events (Figure S10). With medium RhoGEF activation (1.2 J/cm^2), Src induces FA disassembly, and ROCK-mediated contractility assists in FA removal, whereas, with high RhoGEF activation (11 J/cm^2), Src function is counteracted and ROCK stabilizes FAs (Figure S10).

DISCUSSION

In this study, we developed a single-chain photoswitchable activator of RhoA using a photodissociable dimeric variant of the fluorescent protein Dronpa. Using psRhoGEF to rapidly and selectively activate RhoA, we confirmed that acute RhoA activation can induce FA disassembly in a dose-specific manner and dissected downstream pathways involved in this response. We found that Src kinase is required for RhoA-induced FA disassembly, but Src activation at FAs is selectively induced by submaximal levels of RhoA. Finally, inhibition of Src activity can switch the response of FAs to RhoA activity from disassembly to enlargement. These results elucidate a specific role of Src in

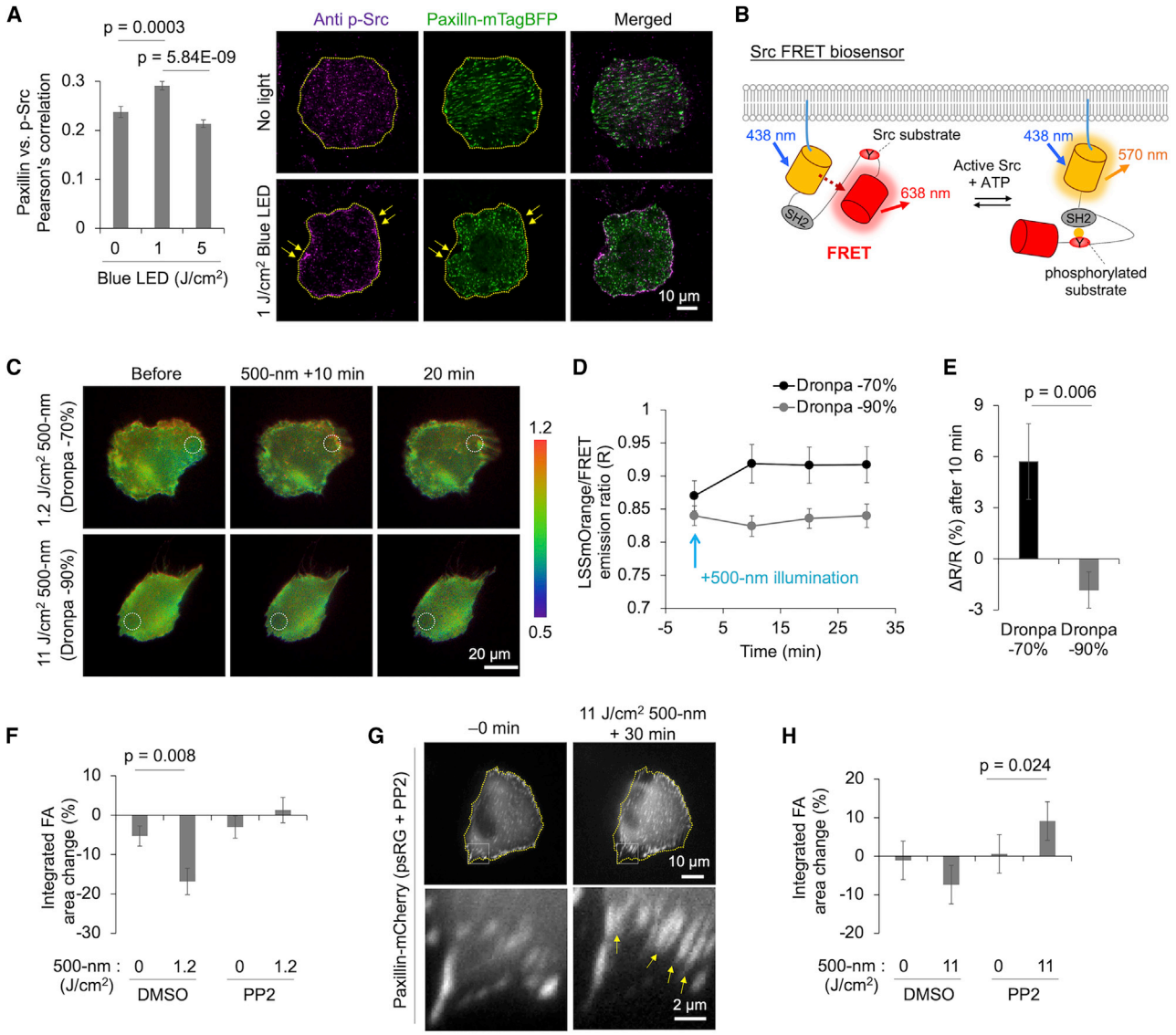

Figure 5. RhoA-mediated FA disassembly involves dose-specific Src activation at FAs

(A) Co-localization of paxillin-mTagBFP and p-Src after different levels of psRhoGEF illumination in U87-MG cells as assessed by immunostaining. Differences between Pearson's correlation coefficients were analyzed by two tailed Student's t test (n = 15, 16, or 12). Representative images are shown on the right. Scale bar, 10 μm.

(B) Schematic of a membrane-targeted Src biosensor (Seong et al., 2009) with LSSmOrange and mKate2 as a FRET pair. In the default state, strong FRET is detected between LSSmOrange and mKate2 (left). Activated Src phosphorylates the substrate peptide (labeled with a red Y), which then binds the SH2 domain, causing a large conformational change and a FRET decrease.

(C) Representative time-lapse images of the Src biosensor in response to different illumination levels in U87-MG cells stably expressing psRhoGEF. Scale bar, 20 μm.

(D) Mean LSSmOrange/FRET emission ratio changes (n = 14 and 16 for 1.2 and 11 J/cm^2, respectively).

(E) Ratio changes at 10 min were compared between light doses by two-tailed Student's t test.

(F) FA area change 30 min after 1.2 J/cm^2 of cyan light or no light in psRhoGEF-expressing cells pre-treated for 30 min with DMSO or 10 μM PP2 (p = 0.008, two-tailed Student's t test; n = 71, 26, 56, or 37). FA area was calculated using the FAAS (Berginski and Gomez, 2013).

(G) Representative images of FAs (paxillin-mCherry) in psRhoGEF-expressing U87-MG cells before and 30 min after 11 J/cm^2 cyan light, after 30-min pre-incubation with 10 μM PP2. Peripheral FAs in the boxed areas are shown with higher magnification in the lower panels. Scale bars, 10 or 2 μm.

(H) FA area change 30 min after 11 J/cm^2 of cyan light or no light in psRhoGEF-expressing cells pre-treated for 30 min with DMSO or 10 μM PP2 (p = 0.024, two-tailed Student's t test, n = 26, 24, 25, or 23). Strong RhoA activation caused an increase in overall FA area.

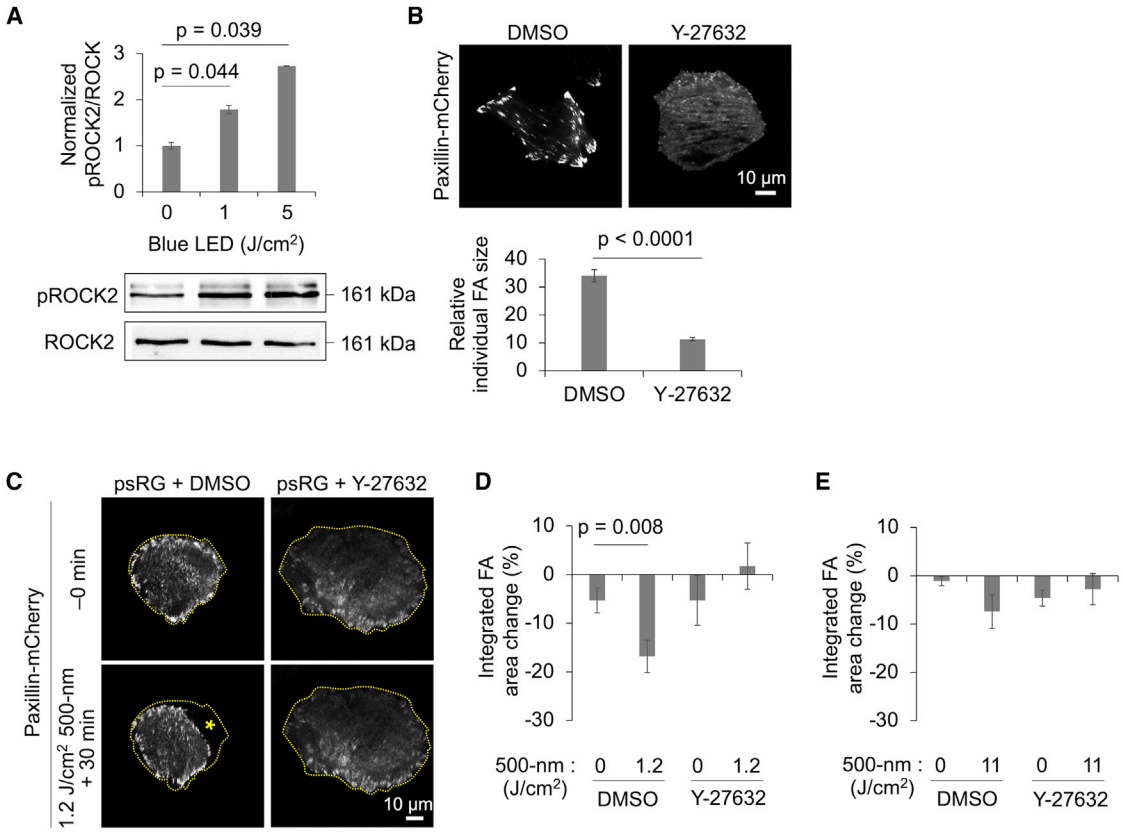

Figure 6. ROCK activity and actomyosin contractility are required for FA assembly and disassembly

(A) Levels of phosphorylated-ROCK2 (p-ROCK2) in U87-MG cells expressing psRhoGEF before or after different light doses by immunostaining. Blue LED light was applied at the indicated energy densities. pROCK2 was quantified relative to ROCK2. ANOVA was performed, and statistical differences were calculated by post-hoc Dunnett's test (n = 4).

(B) Representative FA images labeled by paxillin-mCherry (top panels) and quantification of FA sizes (bottom panels) in psRhoGEF-expressing cells incubated with DMSO or 10 μM ROCK inhibitor Y-27632 for 30 min. FA area was calculated using the FAAS (Berginski and Gomez, 2013). Statistical differences were calculated by two tailed Student's t test (n = 18 or 23). Scale bar, 10 μm.

(C) Representative images in psRhoGEF-expressing cells preincubated with DMSO or Y-27632 for 30 min at a 30-min interval without or with 1.2 J/cm^2 of illumination. Scale bar, 10 μm.

(D) Associated changes in total FA area (p = 0.008 by two-tailed Student's t test; n = 71, 26, 23, or 21).

(E) Quantification of total FA change in psRhoGEF-expressing cells preincubated with DMSO or Y-27632 for 30 min at a 30-min interval without or with 11 J/cm^2 of illumination (n = 26, 24, 23, or 22).

RhoA-induced FA disassembly and explain how a biochemical signal can produce opposite outcomes depending on signal amplitude and context. It has been suggested that RhoA has different affinity for each downstream effector; RhoA-mDia and RhoA-ROCK complexes have dissociation constants of 6 and 130 nM, respectively (Narumiya et al., 2009). Thus, submaximal concentrations of active RhoA could selectively activate mDia signaling to Src to induce FA disassembly, whereas high RhoA activity may preferentially activate ROCK to promote actomyosin contractility and FA growth. This model suggests that, in addition to RhoA signal amplitude, FA responses in a cell, or parts of a cell, can be modulated by the activity of other regulators of Src and ROCK.

Although functions of RhoA effectors such as ROCK and mDia in FA growth are well characterized (Burridge and Guilluy, 2016), their roles in FA disassembly have been much less studied. For example, FAs shrink or disappear upon inhibition or depletion of ROCK or mDia (Burridge and Guilluy, 2016). The same proteins have been implicated in FA disassembly based on more complex experiments examining rates of FA disassembly at the lagging edge of migrating cells, where FA disassembly can be reliably observed (Burridge and Guilluy, 2016; Lock et al., 2012; Parsons et al., 2010; Webb et al., 2004; Yamana et al., 2006). However, ongoing migration requires polarization of cells and FA assembly at the leading edge, processes that also require RhoA effectors (Parsons et al., 2010). Thus, chronic and global manipulations of these pathways cannot unambiguously reveal direct roles of RhoA effectors in FA disassembly versus secondary roles by affecting migration. In contrast to use of dominant-negative or constitutively active constructs or stimulation by extracellular stimuli, optical induction of psRhoGEF allows control of endogenous RhoA with tight

temporal control and without activation of other signaling pathways. This allows immediate responses to RhoA activation to be assessed without feedback or crosstalk.

Our observation that cells can convert rheostatic RhoA signaling into opposite FA responses provides an example of how the same signal can be used to create distinct outcomes via amplitude encoding. Interestingly, RhoA may also be involved in the ability of neurons to respond to different concentrations of the chemokine SDF-1α by either enhancing or inhibiting axonal growth. While both responses require RhoA, enhancement or inhibition requires mDia or ROCK, respectively (Arakawa et al., 2003). However, in these earlier experiments, individual signaling proteins could not be specifically activated, and biological pathways could only be activated by SDF-1α application, whose downstream effects have not been comprehensively mapped. Thus, whether RhoA activity levels determine the response switch or whether the SDF-1α receptor CXCR4 engages different signaling pathways depending on the size of the activated receptor population could not be ascertained. In our current experiments, by directly modulating RhoA activity levels, we were able to determine that RhoA activity amplitude alone is sufficient to drive a switch between two different outcomes.

Another case of opposing responses resulting from different levels of activity of a single protein is provided by another family of small GTPases, the Ras family. Here a low level of Ras activity induces proliferation of mammalian cells through activation of various effectors that promote protein synthesis and transcription of growth-promoting genes, whereas a high level of Ras activity caused by Ras mutation or amplification induces transcription of the cell cycle inhibitor p16 and growth arrest (Dimauro and David, 2010). However, this switch in Ras function occurs only upon mutation or amplification of Ras, a permanent genetic change, and, thus, cannot be dynamically regulated. In contrast, the amplitude modulation of RhoA function we observed provides a mechanism by which pathway inputs can dynamically select between alternative outputs. In other known examples of amplitude-dependent outcomes, it has not yet been demonstrated that amplitude modulation of a single intracellular signal can select between two induced outcomes (as opposed to a simple response versus a no-response decision). For example, in mammalian chondrocytes and *Xenopus* embryos, a low level of extracellular Wnt activates calcium release from internal stores, whereas a high level activates the β-catenin pathway (Kestler and Kuhl, 2011). However, the mechanism behind this switch appears to be concentration-dependent utilization of different Wnt receptors, and thus, response selection occurs outside of rather than in the cell. In *Drosophila* embryos, different concentrations of an epidermal growth factor homolog produce different levels of Ras activity, leading to a binary choice between transcription or no transcription (Sagner and Briscoe, 2017), but in this case, one of the outcomes is identical to the default unstimulated state.

This study demonstrates that the design of the Dronpa-based photoswitchable GEFs is generalizable from the previously developed psCdc42GEF to psRhoGEF. These optobiochemical tools should be broadly useful for investigating the functions of endogenous small Rho GTPases. For example, experiments comparing the functions of these GTPases can now be performed with a consistent set of conditions. Photoswitchable GEFs should also enable spatiotemporal control of the combination of Rho GTPases through expression of the corresponding combination of photoswitchable GEFs. These single-chain photoswitchable GEFs enable simpler experimental designs compared with methods that utilize light-induced heterodimerization to recruit GEFs to the membrane (O'Neill et al., 2016; Valon et al., 2017; Wagner and Glotzer, 2016). Unlike optically controlled fusion proteins of Rho GTPases, these photoswitchable GEFs should avoid artifactual effects arising from titration of a limiting number of RhoGDI molecules (Boulter and Garcia-Mata, 2010). We thus expect that Dronpa-based design of photoswitchable GEFs will be widely useful for investigating the functions of Rho-family GTPases with high spatiotemporal specificity and minimal perturbation to signaling networks.

Limitations of the study

This study has demonstrated that RhoA signal amplitude can specify different outcomes in FA morphology, and on the role of Src in regulating the choice, but it primarily involves studies in HEK293 cells and U87-MG cells. It remains to be determined what other cell types also regulate FA growth and disassembly using these mechanisms. The study also raises implications for how Src inhibitors might decrease the metastatic potential of cancer cells by altering adhesive strength, but these questions remain to be answered. Finally, whether local amplitude regulation of RhoA activation can be used to specifically induce FA growth in one part of the cell and FA disassembly in another part and therefore purposefully induce directional cell migration is an interesting possibility that remains to be addressed.

STAR★METHODS

Detailed methods are provided in the online version of this paper and include the following:

- KEY RESOURCES TABLE
- RESOURCE AVAILABILITY
  - Lead contact
  - Materials availability
  - Data and code availability
- METHOD DETAILS
  - Cell culture and reagents
  - DNA construction and plasmids
  - Live-cell imaging and analysis
  - Rho GTPase pull-down assay
  - Western blotting
  - Immunostaining
- QUANTIFICATION AND STATISTICAL ANALYSIS

SUPPLEMENTAL INFORMATION

Supplemental information can be found online at https://doi.org/10.1016/j.celrep.2022.111080.

ACKNOWLEDGMENTS

This work is supported by KIST institutional grant 2E31523, Samsung Research Funding and Incubation Center of Samsung Electronics under

project SRFC-TC2003-02, National Research Foundation of Korea (NRF) grant 2021R1A2C1093429 (to J.S.), the Stanford Department of Bioengineering (to A.L.-R.), and an NIH Pioneer Award 5DP1GM111003 (to L.N., X.X.Z., and M.Z.L.).

AUTHOR CONTRIBUTIONS

J.S. and M.Z.L. designed the research. J.S., J.J., H.N.L., L.N., H.R., X.X.Z., H.C., Y.W.L., and A.L.-R. performed the experiments. J.S., M.Z.L., J.J., H.N.L., L.N., and C.J. analyzed the data. J.S. and M.Z.L. wrote the manuscript.

DECLARATION OF INTERESTS

The authors declare no competing interests.

Received: September 27, 2021
Revised: May 19, 2022
Accepted: June 21, 2022
Published: July 12, 2022

REFERENCES

Amano, M., Chihara, K., Kimura, K., Fukata, Y., Nakamura, N., Matsuura, Y., and Kaibuchi, K. (1997). Formation of actin stress fibers and focal adhesions enhanced by Rho-kinase. Science *275*, 1308–1311. https://doi.org/10.1126/science.275.5304.1308.

Amano, M., Nakayama, M., and Kaibuchi, K. (2010). Rho-kinase/ROCK: a key regulator of the cytoskeleton and cell polarity. Cytoskeleton (Hoboken) *67*, 545–554. https://doi.org/10.1002/cm.20472.

Arakawa, Y., Bito, H., Furuyashiki, T., Tsuji, T., Takemoto-Kimura, S., Kimura, K., Nozaki, K., Hashimoto, N., and Narumiya, S. (2003). Control of axon elongation via an SDF-1α/Rho/mDia pathway in cultured cerebellar granule neurons. J. Cell Biol. *161*, 381–391. https://doi.org/10.1083/jcb.200210149.

Berginski, M.E., and Gomez, S.M. (2013). The Focal Adhesion Analysis Server: a web tool for analyzing focal adhesion dynamics. F1000Res *2*, 68. https://doi.org/10.12688/f1000research.2-68.v1.

Berlew, E.E., Kuznetsov, I.A., Yamada, K., Bugaj, L.J., Boerckel, J.D., and Chow, B.Y. (2021). Single-component optogenetic tools for inducible RhoA GTPase signaling. Adv. Biol. (Weinh) *5*, e2100810. https://doi.org/10.1002/adbi.202100810.

Bielnicki, J.A., Shkumatov, A.V., Derewenda, U., Somlyo, A.V., Svergun, D.I., and Derewenda, Z.S. (2011). Insights into the molecular activation mechanism of the RhoA-specific guanine nucleotide exchange factor, PDZRhoGEF. J. Biol. Chem. *286*, 35163–35175. https://doi.org/10.1074/jbc.M111.270918.

Boulter, E., and Garcia-Mata, R. (2010). RhoGDI: a rheostat for the Rho switch. Small GTPases *1*, 65–68. https://doi.org/10.4161/sgtp.1.1.12990.

Bozza, W.P., Zhang, Y., Hallett, K., Rosado, L.A.R., and Zhang, B. (2015). RhoGDI deficiency induces constitutive activation of Rho GTPases and COX-2 pathways in association with breast cancer progression. Oncotarget *6*, 32723–32736. https://doi.org/10.18632/oncotarget.5416.

Bugaj, L.J., Choksi, A.T., Mesuda, C.K., Kane, R.S., and Schaffer, D.V. (2013). Optogenetic protein clustering and signaling activation in mammalian cells. Nat. Methods *10*, 249–252. https://doi.org/10.1038/nmeth.2360.

Burridge, K., and Guilluy, C. (2016). Focal adhesions, stress fibers and mechanical tension. Exp. Cell Res. *343*, 14–20. https://doi.org/10.1016/j.yexcr.2015.10.029.

Carragher, N.O., and Frame, M.C. (2004). Focal adhesion and actin dynamics: a place where kinases and proteases meet to promote invasion. Trends Cell Biol. *14*, 241–249. https://doi.org/10.1016/j.tcb.2004.03.011.

Dimauro, T., and David, G. (2010). Ras-induced senescence and its physiological relevance in cancer. Curr. Cancer Drug Targets *10*, 869–876. https://doi.org/10.2174/156800910793357998.

Fritz, R.D., Letzelter, M., Reimann, A., Martin, K., Fusco, L., Ritsma, L., Ponsioen, B., Fluri, E., Schulte-Merker, S., van Rheenen, J., and Pertz, O. (2013). A versatile toolkit to produce sensitive FRET biosensors to visualize signaling in time and space. Sci. Signal. *6*, rs12. https://doi.org/10.1126/scisignal.2004135.

Glantz, S.T., Berlew, E.E., and Chow, B.Y. (2019). Synthetic cell-like membrane interfaces for probing dynamic protein-lipid interactions. Methods Enzymol. *622*, 249–270. https://doi.org/10.1016/bs.mie.2019.02.015.

Glantz, S.T., Berlew, E.E., Jaber, Z., Schuster, B.S., Gardner, K.H., and Chow, B.Y. (2018). Directly light-regulated binding of RGS-LOV photoreceptors to anionic membrane phospholipids. Proc. Natl. Acad. Sci. USA *115*, E7720–E7727. https://doi.org/10.1073/pnas.1802832115.

Heasman, S.J., and Ridley, A.J. (2010). Multiple roles for RhoA during T cell transendothelial migration. Small GTPases *1*, 174–179. https://doi.org/10.4161/sgtp.1.3.14724.

Jaiswal, M., Gremer, L., Dvorsky, R., Haeusler, L.C., Cirstea, I.C., Uhlenbrock, K., and Ahmadian, M.R. (2011). Mechanistic insights into specificity, activity, and regulatory elements of the regulator of G-protein signaling (RGS)-containing Rho-specific guanine nucleotide exchange factors (GEFs) p115, PDZ-RhoGEF (PRG), and leukemia-associated RhoGEF (LARG). J. Biol. Chem. *286*, 18202–18212. https://doi.org/10.1074/jbc.M111.226431.

Kestler, H.A., and Kühl, M. (2011). Generating a Wnt switch: it's all about the right dosage. J. Cell Biol. *193*, 431–433. https://doi.org/10.1083/jcb.201103167.

Kristelly, R., Gao, G., and Tesmer, J.J. (2004). Structural determinants of RhoA binding and nucleotide exchange in leukemia-associated Rho guanine-nucleotide exchange factor. J. Biol. Chem. *279*, 47352–47362. https://doi.org/10.1074/jbc.M406056200.

Lock, F.E., Ryan, K.R., Poulter, N.S., Parsons, M., and Hotchin, N.A. (2012). Differential regulation of adhesion complex turnover by ROCK1 and ROCK2. PLoS One *7*, e31423. https://doi.org/10.1371/journal.pone.0031423.

Luo, L. (2000). Rho GTPases in neuronal morphogenesis. Nat. Rev. Neurosci. *1*, 173–180. https://doi.org/10.1038/35044547.

Machacek, M., Hodgson, L., Welch, C., Elliott, H., Pertz, O., Nalbant, P., Abell, A., Johnson, G.L., Hahn, K.M., and Danuser, G. (2009). Coordination of Rho GTPase activities during cell protrusion. Nature *461*, 99–103. https://doi.org/10.1038/nature08242.

Machiyama, H., Hirata, H., Loh, X.K., Kanchi, M.M., Fujita, H., Tan, S.H., Kawauchi, K., and Sawada, Y. (2014). Displacement of p130Cas from focal adhesions links actomyosin contraction to cell migration. J. Cell Sci. *127*, 3440–3450. https://doi.org/10.1242/jcs.143438.

Meenderink, L.M., Ryzhova, L.M., Donato, D.M., Gochberg, D.F., Kaverina, I., and Hanks, S.K. (2010). P130Cas Src-binding and substrate domains have distinct roles in sustaining focal adhesion disassembly and promoting cell migration. PLoS One *5*, e13412. https://doi.org/10.1371/journal.pone.0013412.

Michaelson, D., Silletti, J., Murphy, G., D'Eustachio, P., Rush, M., and Philips, M.R. (2001). Differential localization of Rho GTPases in live cells: regulation by hypervariable regions and RhoGDI binding. J. Cell Biol. *152*, 111–126. https://doi.org/10.1083/jcb.152.1.111.

Narumiya, S., Tanji, M., and Ishizaki, T. (2009). Rho signaling, ROCK and mDia1, in transformation, metastasis and invasion. Cancer Metastasis Rev. *28*, 65–76. https://doi.org/10.1007/s10555-008-9170-7.

Nobes, C.D., and Hall, A. (1995). Rho, rac, and cdc42 GTPases regulate the assembly of multimolecular focal complexes associated with actin stress fibers, lamellipodia, and filopodia. Cell *81*, 53–62. https://doi.org/10.1016/0092-8674(95)90370-4.

Oakes, P.W., Beckham, Y., Stricker, J., and Gardel, M.L. (2012). Tension is required but not sufficient for focal adhesion maturation without a stress fiber template. J. Cell Biol. *196*, 363–374. https://doi.org/10.1083/jcb.201107042.

Oleksy, A., Opaliński, Ł., Derewenda, U., Derewenda, Z.S., and Otlewski, J. (2006). The molecular basis of RhoA specificity in the guanine nucleotide exchange factor PDZ-RhoGEF. J. Biol. Chem. *281*, 32891–32897. https://doi.org/10.1074/jbc.M606220200.

O'Neill, P.R., Kalyanaraman, V., and Gautam, N. (2016). Subcellular optogenetic activation of Cdc42 controls local and distal signaling to drive immune cell migration. Mol. Biol. Cell *27*, 1442–1450. https://doi.org/10.1091/mbc.E15-12-0832.

Parsons, J.T., Horwitz, A.R., and Schwartz, M.A. (2010). Cell adhesion: integrating cytoskeletal dynamics and cellular tension. Nat. Rev. Mol. Cell Biol. *11*, 633–643. https://doi.org/10.1038/nrm2957.

Paterson, H.F., Self, A.J., Garrett, M.D., Just, I., Aktories, K., Hall, A., and HAll, A. (1990). Microinjection of recombinant p21rho induces rapid changes in cell morphology. J. Cell Biol. *111*, 1001–1007. https://doi.org/10.1083/jcb.111.3.1001.

Pertz, O., Hodgson, L., Klemke, R.L., and Hahn, K.M. (2006). Spatiotemporal dynamics of RhoA activity in migrating cells. Nature *440*, 1069–1072. https://doi.org/10.1038/nature04665.

Ren, X.D., Kiosses, W.B., Sieg, D.J., Otey, C.A., Schlaepfer, D.D., and Schwartz, M.A. (2000). Focal adhesion kinase suppresses Rho activity to promote focal adhesion turnover. J. Cell Sci. *113*, 3673–3678.

Ridley, A.J., Paterson, H.F., Johnston, C.L., Diekmann, D., and Hall, A. (1992). The small GTP-binding protein rac regulates growth factor-induced membrane ruffling. Cell *70*, 401–410. https://doi.org/10.1016/0092-8674(92)90164-8.

Rossman, K.L., Der, C.J., and Sondek, J. (2005). GEF means go: turning on RHO GTPases with guanine nucleotide-exchange factors. Nat. Rev. Mol. Cell Biol. *6*, 167–180. https://doi.org/10.1038/nrm1587.

Sagner, A., and Briscoe, J. (2017). Morphogen Interpretation: Concentration, Time, Competence, and Signaling Dynamics, *6* (Wiley Interdiscip Rev Dev Biol). https://doi.org/10.1002/wdev.271.

Sawada, Y., Tamada, M., Dubin-Thaler, B.J., Cherniavskaya, O., Sakai, R., Tanaka, S., and Sheetz, M.P. (2006). Force sensing by mechanical extension of the Src family kinase substrate p130Cas. Cell *127*, 1015–1026. https://doi.org/10.1016/j.cell.2006.09.044.

Seong, J., and Lin, M.Z. (2021). Optobiochemistry: genetically encoded control of protein activity by light. Annu. Rev. Biochem. *90*, 475–501. https://doi.org/10.1146/annurev-biochem-072420-112431.

Seong, J., Lu, S., Ouyang, M., Huang, H., Zhang, J., Frame, M.C., and Wang, Y. (2009). Visualization of Src activity at different compartments of the plasma membrane by FRET imaging. Chem. Biol. *16*, 48–57. https://doi.org/10.1016/j.chembiol.2008.11.007.

Seong, J., Ouyang, M., Kim, T., Sun, J., Wen, P.C., Lu, S., Zhuo, Y., Llewellyn, N.M., Schlaepfer, D.D., Guan, J.L., et al. (2011). Detection of focal adhesion kinase activation at membrane microdomains by fluorescence resonance energy transfer. Nat. Commun. *2*, 406. https://doi.org/10.1038/ncomms1414.

Seong, J., Tajik, A., Sun, J., Guan, J.L., Humphries, M.J., Craig, S.E., Shekaran, A., García, A.J., Lu, S., Lin, M.Z., et al. (2013). Distinct biophysical mechanisms of focal adhesion kinase mechanoactivation by different extracellular matrix proteins. Proc. Natl. Acad. Sci. USA *110*, 19372–19377. https://doi.org/10.1073/pnas.1307405110.

Snyder, J.T., Worthylake, D.K., Rossman, K.L., Betts, L., Pruitt, W.M., Siderovski, D.P., Der, C.J., and Sondek, J. (2002). Structural basis for the selective activation of Rho GTPases by Dbl exchange factors. Nat. Struct. Biol. *9*, 468–475. https://doi.org/10.1038/nsb796.

Stricker, J., Beckham, Y., Davidson, M.W., and Gardel, M.L. (2013). Myosin II-mediated focal adhesion maturation is tension insensitive. PLoS One *8*, e70652. https://doi.org/10.1371/journal.pone.0070652.

Valon, L., Marín-Llauradó, A., Wyatt, T., Charras, G., and Trepat, X. (2017). Optogenetic control of cellular forces and mechanotransduction. Nat. Commun. *8*, 14396. https://doi.org/10.1038/ncomms14396.

Wagner, E., and Glotzer, M. (2016). Local RhoA activation induces cytokinetic furrows independent of spindle position and cell cycle stage. J. Cell Biol. *213*, 641–649. https://doi.org/10.1083/jcb.201603025.

Wang, H., Vilela, M., Winkler, A., Tarnawski, M., Schlichting, I., Yumerefendi, H., Kuhlman, B., Liu, R., Danuser, G., and Hahn, K.M. (2016). LOVTRAP: an optogenetic system for photoinduced protein dissociation. Nat. Methods *13*, 755–758. https://doi.org/10.1038/nmeth.3926.

Wang, W., Liu, Y., and Liao, K. (2011). Tyrosine phosphorylation of cortactin by the FAK-Src complex at focal adhesions regulates cell motility. BMC Cell Biol. *12*, 49. https://doi.org/10.1186/1471-2121-12-49.

Webb, D.J., Donais, K., Whitmore, L.A., Thomas, S.M., Turner, C.E., Parsons, J.T., and Horwitz, A.F. (2004). FAK-Src signalling through paxillin, ERK and MLCK regulates adhesion disassembly. Nat. Cell Biol. *6*, 154–161. https://doi.org/10.1038/ncb1094.

Wolfenson, H., Bershadsky, A., Henis, Y.I., and Geiger, B. (2011). Actomyosin-generated tension controls the molecular kinetics of focal adhesions. J. Cell Sci. *124*, 1425–1432. https://doi.org/10.1242/jcs.077388.

Wong, K., Pertz, O., Hahn, K., and Bourne, H. (2006). Neutrophil polarization: spatiotemporal dynamics of RhoA activity support a self-organizing mechanism. Proc. Natl. Acad. Sci. USA *103*, 3639–3644. https://doi.org/10.1073/pnas.0600092103.

Wu, Y.I., Frey, D., Lungu, O.I., Jaehrig, A., Schlichting, I., Kuhlman, B., and Hahn, K.M. (2009). A genetically encoded photoactivatable Rac controls the motility of living cells. Nature *461*, 104–108. https://doi.org/10.1038/nature08241.

Yamana, N., Arakawa, Y., Nishino, T., Kurokawa, K., Tanji, M., Itoh, R.E., Monypenny, J., Ishizaki, T., Bito, H., Nozaki, K., et al. (2006). The Rho-mDia1 pathway regulates cell polarity and focal adhesion turnover in migrating cells through mobilizing Apc and c-Src. Mol. Cell Biol. *26*, 6844–6858. https://doi.org/10.1128/MCB.00283-06.

Zhou, X.X., Chung, H.K., Lam, A.J., and Lin, M.Z. (2012). Optical control of protein activity by fluorescent protein domains. Science *338*, 810–814. https://doi.org/10.1126/science.1226854.

Zhou, X.X., Fan, L.Z., Li, P., Shen, K., and Lin, M.Z. (2017). Optical control of cell signaling by single-chain photoswitchable kinases. Science *355*, 836–842. https://doi.org/10.1126/science.aah3605.

STAR★METHODS

KEY RESOURCES TABLE

REAGENT or RESOURCE	SOURCE	IDENTIFIER
Antibodies		
Mouse monoclonal anti-Rho	EMD Millipore	Cat#05-778; RRID: AB_309989
Mouse monoclonal anti-GAPDH	Santa Cruz Biotechnology	Cat#sc-47724; PRID: AB_627678
Rabbit polyclonal anti-phospho-Src (Tyr416)	Cell Signaling Technology	Cat#2101; RRID: AB_331697
Goat anti-rabbit IgG conjugated to Alexa-fluor 594	Thermo Fisher Scientific	Cat#A-11037; RRID: AB_2534095
Rabbit polyclonal anti-phospho-ROCK2	Abcam	Cat#ab228008
Rabbit polyclonal anti-ROCK2	Cell Signaling Technology	Cat#8236; RRID: AB_10829468
Chemicals, peptides, and recombinant proteins		
Non-essential amino acid (NEAA)	Gibco	Cat#11140-050
Penicillin-streptomycin solution	Corning	Cat#30-002-CIPe
FBS	Hyclone	Cat#SH30070.01
Cell lysis buffer	Cell signaling	Cat#9803S
Phenylmethanesulfonyl fluoride (PMSF)	Sigma Aldrich	Cat#P7626; CAS: 329-98-6
Sodium fluoride (NaF)	Sigma Aldrich	Cat#201154; CAS: 7681-49-4
Protease inhibitor cocktail	Cytoskeleton, Inc	Cat#PIC02
Lipofectamine 2000 transfection reagent	Invitrogen	Cat#11668019
PP2	Sigma Aldrich	Cat#529573; CAS: 172889-27-9
Y-27632	Sigma Aldrich	Cat#Y0503; CAS: 146986-50-7
Fibronectin Bovine Protein	Gibco	Cat#33010018
DMSO	Sigma Aldrich	Cat#D2650
Critical commercial assays		
Rho activation assay kit	EMD Millipore	Cat#17-294
Experimental models: Cell lines		
HEK293A human embryonic kidney cell line	Invitrogen	Cat#R70507
U87-MG human glioblastoma cell line	Korean Cell Line Bank	Cat#30014
U87-MG psRhoGEF stable cell line	This study	N/A
Recombinant DNA		
mCardinal-Lifeact-7	Addgene	Plasmid #54663
DronpaN-PRG DH-GSS4-DronpaN	This study	N/A
pdDronpaM-PRG DH-GSS4-pdDronpaM	This study	N/A
pdDronpaM-PRG DHPH-GSS3-pdDronpaM	This study	N/A
pdDronpaV-PRG DHPH-GSS3-pdDronpaV	This study	N/A
pdDronpaV-PRG DHPH-GSS2-pdDronpaV	This study	N/A
pdDronpaV-PRG DHPH-GSS1-pdDronpaV	This study	N/A
pdDronpa1-PRG DHPH-GSS3-pdDronpa1	This study	N/A
pdDronpa1-PRG DHPH-GSS2-pdDronpa1	This study	N/A
pdDronpa1-PRG DHPH-GSS1-pdDronpa1	This study	N/A
pdDronpa1-PRG DHPH-GSS3-pdDronpa1 N145K	This study	N/A
pdDronpa1-PRG DHPH-GSS2-pdDronpa1 N145K	This study	N/A
pdDronpa1-PRG DHPH-GSS1-pdDronpa1 N145K	This study	N/A
LSSmOrange-RBD-mKate2-WT RhoA	This study	N/A
LSSmOrange-RBD-mKate2-T17N RhoA	This study	N/A
LSSmOrange-RBD-mKate2-G14V RhoA	This study	N/A
p2A-EGFP	This study	N/A

(*Continued on next page*)

Continued

REAGENT or RESOURCE	SOURCE	IDENTIFIER
EGFP-p2A-ITSN DH	This study	N/A
EGFP-p2A-Tiam DH	This study	N/A
EGFP-p2A-PRG DHPH	This study	N/A
Dronpa N145K	This study	N/A
PRG DHPH-Dronpa N145K	This study	N/A
pdDronpaV-PRG DH(R868G)PH-GSS1-pdDronpaV	This study	N/A
Paxillin-mTagBFP	This study	N/A
Paxillin-mCherry	Addgene	Plasmid #55114
Vinculin-mCherry	Addgene	Plasmid #55159
Lyn-LSSmOrange-SH2-Src substrate-mKate2	This study	N/A
OptoGEF-RhoA and CIBN-CAAX	Addgene	Plasmid #89481, 79574
PR-GEF and Stargazin-GFP-LOVpep	Addgene	Plasmid #80407, 80406
Software and algorithms		
GraphPad Prism 8	GraphPad software	https://www.graphpad.com/scientific-software/prism/
NIS-Elements AR 4.5 (Advanced Research)	Nikon	https://www.microscope.healthcare.nikon.com/products/software/nis-elements/nis-elements-advanced-research
MetaMorph software	Molecular Devices	N/A
Image Lab 6.0 software	Bio-Rad	https://www.bio-rad.com/product/image-lab-software
Focal Adhesion Analysis Server (FAAS)	(Berginski and Gomez, 2013)	https://faas.bme.unc.edu/

RESOURCE AVAILABILITY

Lead contact

Further information and requests for resources and reagents should be directed to and will be fulfilled by the lead contact, Jihye Seong (jseong@kist.re.kr).

Materials availability

All unique materials generated in this study are available from the lead contact with a completed Materials Transfer Agreement as applicable.

Data and code availability

All data reported in this paper will be shared by the lead contact upon request.
This paper does not report original code.
Any additional information required to reanalyze the data reported in this paper is available from the lead contact upon request.

METHOD DETAILS

Cell culture and reagents

HEK293A cells were maintained in Dulbecco's modified Eagle medium (DMEM) supplemented with 2 mM L-glutamine (GE Healthcare Life Sciences), 10% fetal bovine serum (FBS, GE Healthcare Life Sciences), 1 unit/mL penicillin (Corning), 100 g/mL streptomycin (Corning), non-essential amino acid (NEAA, Life Technologies), and 1 mM sodium pyruvate (Life Technologies). U87-MG cells were maintained in Dulbecco's modified Eagle medium (DMEM) supplemented with 2 mM L-glutamine, 10% FBS, 1 unit/mL penicillin, 100 g/mL streptomycin, and 1 mM sodium pyruvate. Cells were cultured in a humidified 95% air, 5% CO_2 incubator at 37°C. For the transient transfection, we used Lipofectamine 2000 (Invitrogen) or lentiviruses which were prepared by KIST Virus Facility. Src inhibitor PP2, ROCK inhibitor Y-27632 were purchased from Sigma.

DNA construction and plasmids

Plasmids were constructed by standard molecular biology methods such as polymerase chain reaction (PCR) and In-fusion cloning (Clontech). Mutations for specific amino acids were generated by overlap-extension PCR. All cloning junctions and PCR products were verified by sequencing process. The pcDNA3 vector was used for the expression in mammalian cells, and pLL3.7 vector

was used for virus production at KIST virus facility. Full plasmid sequences are available upon request, and main constructs will be available in Addgene after publication.

Live-cell imaging and analysis

For all imaging experiments, cover-glass-bottom dishes (SPL Life Sciences) were prepared by coating 10 μg/mL or indicated concentrations (for psRacGEF experiments) of fibronectin bovine protein (Gibco) for at least 2 h at 37°C. Cells expressing each construct were cultured on fibronectin-coated cover-glass-bottom dishes and incubated in media with 0.5% FBS overnight before imaging experiment. During imaging, cells were kept in the imaging chamber maintained with 5% CO_2 and 37°C (Live Cell Instruments). Images were collected by a Nikon Ti-E inverted microscope with Nikon C-LHGFI HG Mercury lamp and a cooled charge-coupled device camera. Cell imaging videos were produced with MetaMorph program (Molecular Devices).

Dronpa variants were imaged with a 1/8 neutral density (ND8) filter, 482/35-nm excitation filter, 506-nm dichroic mirror, 536/40-nm emission filter, and 200 ms of exposure time. mCardinal-tagged Lifeact was imaged with a 1/4 neutral density (ND 4) filter, 531/40-nm excitation filter, 562-nm dichroic mirror, 593/52-nm emission filter, and 200 ms of exposure time. Time-lapse images of Lifeact were obtained every one-minute, for 10 min before photoswitch and for 50 min after photoswitch. Dronpa variants were photoswitched off by illumination on a 100× oil objective (numberical aperture 1.45, working distance 0.13 mm, Nikon) using the same excitation and dichroic filters as for imaging but without a neutral density filter for 30 s. For different light doses, Dronpa was photoswitched by illumination using a 100× oil objective without a neutral density filter (full dose, ND1), 1/8 (ND8), or 1/32 neutral density (ND32) for 30 s or 10 s. Light doses of 0.06 mJ, 0.6 mJ, and 5.4 mJ were obtained with a photometer (Newport 843-R), then divided by an illumination area of 0.05 mm^2 (measured empirically by photobleaching) to obtain energy density values. For illumination of cell populations before immunostaining, blue LED light was applied to cell culture dishes. As the light spot was larger than the photometer sensor, the energy measured was divided by the sensor area of 1 cm^2 to obtain energy density values.

For the FRET imaging, mKate emission from FRET was imaged by 438/24-nm excitation filter, 593-nm dichroic mirror, 641/75-nm emission filter for 200 ms of exposure time. LSSmOrange emission image was collected with 438/24-nm excitation filter, 562-nm dichroic mirror, 593/40-nm emission filter, for 200 ms of exposure time. After background-subtraction, the pixel-by-pixel ratio images of FRET/LSSmOrange for RhoA biosensor and LSSmOrange/FRET for Src biosensor were calculated by the NIS program. The average emission ratios in total or local cell area (R) or its relative change after stimulation (ΔR/R) were calculated for the statistical analysis of FRET responses.

Total internal reflection fluorescence (TIRF) images of mCherry-tagged paxillin before and after psRhoGEF activation were acquired under Nikon Ti-E inverted microscope equipped with fiber-coupled 488-nm and 561-nm lasers to excite Dronpa and mCherry, respectively. NIS-elements software was used for image acquisition and analysis. Focal adhesion (FA) area for each cell at each time point was automatically calculated using the Focal Adhesion Analysis Server (FAAS) (Berginski and Gomez, 2013). Cells were categorized as showing FA growth or FA shrinkage if total FA area change during the experiment was higher than the standard deviation in the non-stimulated population.

Rho GTPase pull-down assay

U87-MG cells stably infected by lentiviral psRhoGEF were lysed with MLB buffer (EMD Millipore) containing 25 mM, 1mM sodium orthovanadate, and protease inhibitor cocktail tablet (Roche). All samples were quantified and agitated overnight at 4°C with 23 μL of Rhotekin RBD agarose bead (EMD Millipore). Equal amounts of protein were subject to SDS-PAGE and blotted with anti-Rho antibody (3 μg/mL, #05-778, EMD Millipore) or anti-GAPDH antibody (1:1000 dilution, #SC47724, Santa Cruz Biotechnology). We developed western blot membranes with enhanced chemiluminescence (ECL) solution and images were captured with a luminescent image analyzer Amersham Imagequant 800 (Cytiva, USA).

Western blotting

U87-MG cells infected by psRhoGEF containing lentiviruses were cultured for around 30 h and then starved in 0.5% FBS media for overnight. These cells were lysed with cell lysis buffer (Cell signaling) containing 1 mM PMSF, 5 mM NaF, and protease inhibitor cocktail (Cytoskeleton). Equal amounts of protein were subject to SDS-PAGE and blotted with polyclonal anti-phosphorylated ROCK2 antibody (1.3 μg/mL, #ab228008, Abcam) or polyclonal anti-ROCK2 antibody (1:1000 dilution, #8236, Cell Signaling Technology). We developed western blot membranes with enhanced chemiluminescence (ECL) solution and images were captured with a luminescent image analyzer ChemiDoc (Bio-Rad, USA).

Immunostaining

Paxillin-mTagBFP and psRhoGEF co-expressed cells were fixed with 4% paraformaldehyde for 10 min, and permeabilized with 0.1% Triton X-100 for 15 min. Cells were incubated in 5% BSA in PBS for 1 h, and then with rabbit anti-phospho Src Tyr416 (0.69 μg/mL, #2101, Cell Signaling) for overnight at 4°C. After three times of washing with PBS, cells were incubated with goat anti-rabbit antibody conjugated to Alexa-fluor 594 (20 μg/mL, #A-11037, Thermo Fisher Scientific) for 1 h. After three times of washing with PBS for 10 min each, the stained cells were mounted and observed under a TIRF microscopy. For quantifying of p-Src at focal adhesions, the TIRF images of p-Src and paxillin-mTagBFP of the same cell were applied to the Pearson's correlation test via NIS program (Nikon).

QUANTIFICATION AND STATISTICAL ANALYSIS

p values were calculated using two-tailed Student's t-test, the Dunnett's multiple comparisons test, one-way ANOVA test or Tukey's multiple comparisons test (GraphPad Prism 8) for continuous variables, following confirmation of normality calculated by the Shapiro-Wilk test, or using Fisher's exact test for categorical variables.